MULTI-PHASE CFD-CONJUGATE HEAT TRANSFER FOR SPRAY COOLING IN THE NON-BOILING REGIME

by

M. Langari, Z. Yang*, J. F. Dunne**, S. Jafari,
J-P Pirault, C. A. Long, and J. Thalackottore Jose

Department of Engineering and Design
School of Engineering and Informatics
University of Sussex, Falmer, Brighton, BN1 9QT, UK.

* Department of Engineering, College of Engineering and Technology
University of Derby, UK

** Corresponding author: E-mail: j.f.dunne@sussex.ac.uk

SUMMARY

A numerical study is described to predict, in the non-boiling regime, the heat transfer from a circular flat surface cooled by a full-cone spray of water at atmospheric pressure. Simulations based on coupled Computational Fluid Dynamics and Conjugate Heat Transfer are used to predict the detailed features of the fluid flow and heat transfer for three different spray conditions involving three mass fluxes between 3.5 and 9.43 kg/m^{2}s corresponding to spray Reynolds numbers between 82 and 220, based on a 20 mm diameter target surface. A two-phase Lagrange-Eulerian modelling approach is adopted to resolve the spray-film flow dynamics. Simultaneous evaporation and condensation within the fluid film is modelled by solving the mass conservation equation at the film-continuum interface. Predicted heat transfer coefficients on the cooled surface are compared with published experimental data showing good agreement. The spray mass flux is confirmed to be the dominant factor for heat transfer in spray cooling, where single-phase convection within the thin fluid film on the flat surface is identified as the primary heat transfer mechanism. This enhancement of heat transfer, via single-phase convection, is identified to be the result of the discrete random nature of the droplets disrupting the surface thin film.

14 main-section pages (double spaced) 33 references Figures 1 – 8 No Appendices

1. INTRODUCTION

Spray cooling has been the subject of research focused on several important potential application areas [1 - 7]. These applications mainly include cooling in grid power generation systems and power electronics, where in some cases traditional convective cooling methods have reached their physical limitations. The ultimate aim of the current study is an automotive application focusing on robust spray cooling for thermal management of highly-boosted combustion engines used in hybrid electric vehicles. In recent years, a wealth of experimental evidence has been obtained to highlight the benefits of using spray cooling. However, as a method of thermal management, spray cooling has not yet been industrially-applied to any significant degree. The most likely cause for this, is a lack of theoretical understanding of the underlying heat transfer mechanisms. These mechanisms inherently occur at small-scale involving complex interactions of several phenomena such as droplet-break-up, impingement, thin fluid-film formation, convection, conduction, nucleation, and phase-change. The performance of spray cooling is known to depend on many factors including nozzle type, spray volumetric flux, droplet size, spray angle, orifice-to-surface distance, and the degree of fluid 'sub-cooling' [8 - 14].

Despite numerous studies, knowledge of the fundamental heat transfer processes in spray cooling are still limited owing to the complexity of the mechanisms described. Heat transfer models are limited to prediction under specific conditions corresponding to particular experimental test conditions [15]. Experimentally-derived correlations involve a large number of test conditions to achieve an optimum combination of dependent parameters for any particular cooling condition. CFD modelling by contrast can significantly improve the current state-of-the-art prediction capability by including important physical effects. These include droplet momentum and wall impingement, fluid-film thickness, gravity, surface tension, and phase-change, leading to better understanding and more reliable spray cooling simulation and subsequent system design. Spray cooling however occurs over a diverse

range of length-scales involving thousands of droplets that are orders of magnitude smaller in diameter than the target surface length scale. This requires very significant computational power making direct simulation of all aspects of spray cooling quite unfeasible. Alternatively, a Lagrange-Eulerian approach [16] allows the multiple scales associated with spray cooling to be numerically resolved resulting in acceptable simulation times. In this framework, spray formation and droplet dynamics are traced individually (in representative 'parcels') until they impinge on a fluid layer or wall, where mass, momentum, and energy transfer takes place between a droplet and the wall or film [17][18]. A wall-impingement model then accounts for the mass that rebounds, splashes, or adheres to the film, resulting in redistribution of momentum and thermal energy for both the liquid film and any rebounding droplets.

Rehman *et al.* [17] numerically-modelled and simulated a swirling jet flow from a nozzle using the volume-of-fluid method to study spray formation characteristics for several fluids, including water. It was observed that the pressure drop in the spray nozzle increases with flow rate, and that the properties of the liquid have a significant effect on the spray cone angle. Stanton and Rutland [19] developed a two-dimensional wall film model to solve the mass continuity and momentum conservation equations. This includes the effects of spray droplet impingement and splashing using a set of correlations to express the distribution of mass and momentum for the incident droplet as a function of key dimensionless groups. CFD simulations by Sarkar and Selvam [20] showed a significant increase in the ratio of the local transient heat flux to the average heat flux of the thin film within droplet impact cavities. Bai *et al.* [21] developed a spray impingement model for gasoline spray wall impact simulations. The model was assessed by simulating experimental conditions for oblique spray impingement in a wind tunnel, resulting in good agreement between the calculated wall spray characteristics and experimental measurements. Jafari [22] simulated single-phase combined spray and film heat transfer using the Bai-Gosman impingement model [21]. This model applies to a surface temperature below boiling for the fluid spray, where the

error in the predicted heat transfer coefficient was 9%. Youssef [23] used numerical simulations to study rewetting of a hot surface by droplet impingement and found that cooling is improved by increasing spray velocity (owing to increased momentum in the liquid layer impacted by the spray). Simulations also showed that cooling is improved by a reduction in the distance between the nozzle and the hot surface, and by an increase in the spray mass flow rate. Meredith *et al.* [24] developed a model for simulating water film transport over a solid surface and coupled it with a gas-phase solver and spray transport model. This predicted good agreement with experimental measurement for film thickness, velocity, and mass flow rate.

A review of evaporative cooling concepts used in automotive applications suggests a combination of single-phase and fully evaporative cooling may offer the most practical approach to implementation [25]. Pautsch and Shedd [14], from an extensive parametric study of spray cooling using different nozzle patterns, showed that the heat transfer associated with phase change may contribute up to 30% of the total cooling. It was found that systems with the highest peak heat fluxes were obtained when phase change was avoided. It was also suggested that cooling is dominated by single-phase heat transfer in spray systems with liquid film formation on the heated surface. Accurate assessment of spray cooling in the single-phase non-boiling regime is therefore deemed essential for robust spray cooling system design. In the non-boiling regime, the wall temperatures are below the coolant boiling point. Impinging spray droplets on the heated-wall form a liquid film on the surface which is swept away by the stream of coolant droplets removing heat by substantial forced convection, plus some heat removal by evaporation of the liquid film, which is just below saturation temperature. Some experimental studies have examined spray impingement heat transfer in the non-boiling regime [6, 26 - 28]. Kalantari [27] studied the influence of film thickness on droplets-wall interaction and developed a theoretical model to predict the average film thickness as a function of mean Reynolds number, mass flux density

of the impacting droplets, and the average droplet diameter. Experiments by Ciofalo *et al.* [26], using water sprays with mass fluxes between 8 – 80 kg/m^{2}s, indicated that the single-phase heat transfer coefficient depended strongly on the product of mass flux and mean droplet velocity, with no significant dependence on droplet diameter. Karwa *et al.* [28] studied the heat transfer in the non-boiling regime using a pressure atomization nozzle, developing a correlation between Nusselt number and the spray Reynolds number.

Liquid-vapour phase-change can occur at two different states: i) when the temperature is higher than the saturation temperature (based on the local water-vapour concentration) and where evaporation is governed by the partial pressure of the vapour (i.e. until 100% relative humidity is reached), and ii) when the boiling temperature is reached (which is fixed by the air-vapour mixture pressure). None of the CFD studies in the non-boiling regime have considered the effect of film evaporation, which has generally been assumed to make only a small contribution to the total heat transfer. Therefore for accurate heat transfer prediction numerical simulation should include the full effects of both droplet and liquid-film dynamics for both convective and evaporative heat transfer at impinged solid walls. It is also often a requirement to know how the heat transfer occurs within the cooled hot metal and the adjacent coolant fluid. To date, there have been no studies of spray cooling using complete CFD-Conjugate Heat Transfer (CHT) simulations which include evaporation effects in the non-boiling regime. The main objective of the current study is to develop and verify CFD-CHT simulations for non-boiling spray cooling on a flat circular surface as a precursor to application of spray evaporative cooling simulations to the curved geometries under engine-like operating conditions. The geometry and thermal configurations are based on the experimental work of Karwa *et al*. [28]. Simulations are achieved using a finite-volume CFD solver STAR-CCM+ (V11.04) in a Lagrange-Eulerian framework. First, the modelling and simulation approach is described. Then, CFD simulation results are reported, showing a comparison with published experimental measurements.

2. NUMERICAL MODELLING

A description of the modelling features is now given to explain how the particular commercial CFD code used is configured to simulate the particular spray scenario described. This is followed by a formal statement of the equations governing spray evolution with phase change, the boundary conditions, and the meshing details.

Simulations are based on coupling the Lagrangian description of the liquid phase (i.e. a water spray) with an Eulerian description of the gas-phase. The spray comprises 'parcels of droplets' of differing sizes undergoing simultaneous effects as they travel within the mixture of air and water vapour. The segregated solver is used employing a 'Simple' algorithm [29] to couple pressure and velocity. The Lagrangian phase is solved by tracking droplets through the calculated flow field. The spray droplets exchange momentum, mass, and energy, with the Eulerian flow field - their trajectories being computed individually at specified intervals during the fluid phase calculation. The possible aerodynamic-force-induced breakup of droplets in the early stages of the spray leaving the nozzle, are accounted for by the TAB breakup model. Liquid-film build-up resulting from impingement of droplets on the solid surface is resolved in the Eulerian framework. This makes it possible to predict liquid film transportation, heat transfer, and possible disintegration of the film into secondary drops. Interaction of spray droplets with the liquid-filled control volumes i.e. a 'stick or splash' scenario, is dependent on parameters such as the droplet Weber number and velocity. This dependence is predicted by Bai-Gosman model [21]. At low Weber numbers i.e. < 2, droplets stick to the wall contributing to liquid film. At higher Weber numbers, droplets splash, ejecting secondary droplets.

The Standard 3D Reynolds-Averaged Navier-Stokes (RANS) equations, as well as transport equations for mass, energy, and species (air/water vapour) conservation, are solved for the Eulerian-phase as the continuum flow field. The governing equations for conservations of mass, momentum, and energy are:

$$\frac{\partial \rho}{\partial t} + \frac{\partial}{\partial x_i}(\rho u_i) = S_m \tag{1}$$

$$\frac{\partial (\rho u_i)}{\partial t} + \frac{\partial}{\partial x_i}\left(\rho u_i u_j\right) = \rho \overrightarrow{g_j} - \frac{\partial P}{\partial x_j} + \frac{\partial \tau_{ij}}{\partial x_i} + F_j \tag{2}$$

$$\frac{\partial (\rho c_p T)}{\partial t} + \frac{\partial}{\partial x_i}\left(\rho c_p u_i T\right) = \frac{\partial}{\partial x_i}\left(\lambda_{eff}\frac{\partial T}{\partial x_i}\right) + \mu\Phi + S_h \tag{3}$$

where S_m, F_j, S_h are the source terms to include contributions from the Lagrangian-phase and τ_{ij} is the stress tensor defined as:

$$\tau_{ij} = \mu\left(\frac{\partial u_i}{\partial x_j} + \frac{\partial u_j}{\partial x_i} - \frac{2}{3}\delta_{ij}\frac{\partial u_k}{\partial x_k}\right) \tag{4}$$

The terms $\mu\Phi$ and λ_{eff} in the energy equation (3), refer to heat dissipation and effective heat conductivity respectively. Evaporation from the droplets and fluid film (to the continuum field) is included by solving species transport equation for the air and water vapour:

$$\frac{\partial (\rho C_j)}{\partial t} + \frac{\partial}{\partial x_i}\left(\rho u_i C_j\right) = \frac{\partial}{\partial x_i}\left(\rho D_{eff,j}\frac{\partial C_j}{\partial x_i}\right) + S_j \tag{5}$$

where C_j and S_j are the respective mass fraction and source terms. Parameter $D_{eff,j}$ is the effective diffusion coefficient which includes turbulence.

Turbulent interaction between the water spray and the continuum field is simulated using the realisable k-ε turbulence model [30]. The turbulent Prandtl and Schmidt numbers for the continuous phase in the present study are set to 0.9, i.e. the recommended values in STAR_CCM+. For the fluid film layer, conservation equations of mass, momentum, and energy are solved, and integrated over the volume of fluid film in each cell to obtain a set of algebraic equations. Both the quantity of mass impinging on the film, and the source terms for splashing, are computed by the impingement model [21]. Evaporation of the fluid film into the gas phase, and condensation from a gas phase into the fluid film, is modelled by solving the mass conservation equation at the film-continuum interface [29]. Evaporation and condensation is allowed for by component mapping, and by use of the Antoine equation for saturation pressure of water.

Droplets moving in the gaseous field encounter inertia and hydrodynamic drag forces, and can therefore be accelerated or decelerated. The droplet velocity change is thus given by:

$$m_p \frac{d\mathrm{v}_p}{dt} = \mathrm{F}_d + \mathrm{F}_g \tag{6}$$

where v_p is the droplet velocity vector, F_d is the drag from the gas flow on the droplet and F_g is the gravity force. Droplet evaporation resulting from either high-temperature or low humidity partial pressure, leads to vapour diffusion and transport into the continuum field. The rate of evaporation is governed by the concentration difference between the surface and the continuum flow, with corresponding mass rate-of-change given by:

$$\frac{dm_p}{dt} = \pi d^2 g^* (C_s - C_\infty) \tag{7}$$

where C_s is the concentration of the vapour at the droplet surface evaluated by assuming the flow over the surface is saturated, C_∞ is the vapour concentration of the bulk flow obtained by solving the transport equations, and g^* is the mass transfer conductance given by Ranz-Marshal correlation [31]:

$$\frac{g^* d}{D} = 2 + 0.6 Re_d^{0.5} \left(\nu/_D\right)^{0.33} \tag{8}$$

where D is the mass diffusion coefficient of vapour in the bulk flow. The droplet temperature change in the continuum field, owing to both convective heat transfer and latent heat, is computed as:

$$m_p c_p \frac{dT}{dt} = \pi d^2 h (T_\infty - T) + \frac{dm_p}{dt} h_{fg} \tag{9}$$

where h_{fg} is the droplet latent heat and h is the convective heat transfer coefficient given by the empirical correlation [31]:

$$\frac{hd}{\lambda} = 2 + 0.6 Re_d^{0.5} Pr^{0.33} \tag{10}$$

where λ is the heat conductivity of the air/vapour mixtures, and Pr is the Prandtl number.

Evaluation of spray parameters

The water spray is injected at a normal distance from a point located above the centre of the target surface according to the test conditions. From the 10 experimental test cases, varying nozzles and operating conditions, three full-cone spray configurations were chosen for the simulations. Table 1 shows the key parameters for each case. Since the spray cone angle varies with the nozzle type and operating pressure, the experimental nozzle-to-target spacing H was adjusted so that the spray fully inscribed on the target surface.

Table 1. Spray parameters according to experimental conditions used in [28].

Test case	Mass flux, G (Kg/m^2s)	Sauter mean dia, d32 (μm)	Mean droplet velocity, v (m/s)	Nozzle-surface distance, H (mm)	Mass flow rate (kg/s)	Re	We
Case 1	3.50	76.1	54.4	18	0.0011	81.87	3120
Case 2	7.32	137.1	19.9	20	0.0023	175.43	752
Case 3	9.42	118.6	26.3	20	0.0030	220	1136

The experimental heat transfer coefficient *h* is defined as:

$$h = \frac{q}{T_{surface} - T_{inlet}} \tag{11}$$

where q is the heat flux, $T_{surface}$ is the heating surface temperature, and T_{inlet} is the fluid temperature at the entrance of the nozzle. The Reynolds and Weber numbers for the spray are defined as:

$$Re = \frac{GD}{\mu_f} \tag{12}$$

and

$$We = \frac{\rho v^2 d_{32}}{\sigma_f} \tag{13}$$

where D is the diameter of the heated target, G is the mass flux of water based on unit area of the target surface, μ_f is the viscosity of the water, d_{32} is the Sauter mean diameter, and ρ, σ_f, and v are the respective fluid density, surface tension, and mean droplet velocity. The

experimental mean droplet velocity v impacting the surface was estimated using the procedure [28] i.e.:

$$v = \left(\frac{2\nabla P}{\rho}\right)^{1/2} \tag{14}$$

and the Sauter mean diameter was estimated using the correlation [11] as follows:

$$\frac{d_{32}}{d_0} = 3.07\left[\frac{\rho_g^{1/2}\nabla P d_0^{3/2}}{\sigma^{1/2}\mu}\right]^{-0.259} \tag{15}$$

where d_0 is the diameter of the nozzle orifice, μ is liquid dynamic viscosity, and ρ_g is gas density at ambient temperature. The thermo-physical properties of water used in the calculations correspond to the pre-impingement temperature of the water.

Boundary conditions

Given the experimental spray parameters (mass flow rate, droplet size, and velocity), a point spray nozzle is introduced to the domain through a number of computational 'parcels' representing the total population of dispersed phase. The velocity and diameters are given for droplets at the nozzle exit point. Each parcel stream then has part of the total droplets generated. In effect, parcels can be considered as a discretization of the population of dispersed phase in the same way that cells are a discretization of continuous space. As with cells, the number of parcels must be large enough so that the properties of the full population of spray droplets are represented. Calculations involved 1000, 2000, and 3000 parcels to ensure the spray droplet density are adequately represented. An initial air-vapour field is assumed to be air with 5% humidity. The spray flow is assumed to be water at an ambient temperature of 25ºC. The nozzle axis is always kept normal to the surface. A uniform droplet size at the nozzle discharge was used. The droplet diameter at the nozzle exit can be specified with a constant, a log-normal distribution, or some other distribution. A constant value was used corresponding to the experimental conditions (which itself is estimated using a correlation). Uniform velocity distribution is assigned to the spray nozzle inlet to match the

experimental conditions. The spray cone angle was calculated to correspond to the experimental conditions such that spray impact area is just equal to the heater surface. The inlet conditions for turbulence was assumed to have 1% turbulent intensity, and a 1 mm length scale. The outlet boundaries of the main computational domain correspond to constant atmospheric pressure according to the experiment. The walls in the computational domain have non-slip boundary condition and all except the cooled surface are adiabatic. The initial condition for fluid-film was zero thickness. A fixed uniform heat flux was applied at the bottom of the hot surface for all three cases. The experimental heating power was chosen, so that the hot surface temperature was maintained below 95ºC (i.e. a heat flux between 30 - 85 W/cm^2 for the entire range of mass fluxes). The spray chamber pressure was maintained at atmospheric throughout the study.

Geometry and mesh

Figures 1 and 2 show the computational domain, grid, and the boundary conditions used for the simulation of the experimental data published in [28]. The computational domain is discretized using polyhedral cells which includes prism grid layers in the film region with mapped interfaces between the solid domain, fluid film, and air-vapour continuum field. A grid convergence test was undertaken for Case 1 (Table 1) respectively with 98000 and 430000 cells, showing no significant difference in predicted surface temperature when the grid density was increased. The simulation results were therefore obtained using a mesh of 98000 cells.

3. RESULTS AND DISCUSSION

The procedure described in Section 2 is now used to simulate Cases 1, 2, and 3 corresponding to the parameters given in Table 1. By allowing the simulation to run for a sufficiently long time, the surface temperature settles to a steady-state value. Because the mechanism of heat transfer during spray cooling is complex, and the characteristics of spray

(namely the velocity of droplets, droplet size distribution, and droplet number density) have a strong influence on the heat transfer, it is difficult to independently vary each of the spray parameters. This has an impact on how the results are shown.

Figure 3 shows the predicted heat transfer coefficients for Cases 1, 2, and 3, which are in reasonable agreement with the experimental data [28] (i.e. within the range 10 - 20%). Moreover, in respect of the dependence of key parameters in spray cooling, Mudawar & Estes [11] assert that the spray mass flux, not the droplet velocity, is the dominant factor for achieving a particular heat transfer. Both the numerical predictions and experimental data shown in Figure 3 strongly support this assertion that spray mass flux is the dominant factor influencing the heat transfer. In fact, the heat transfer coefficient appears to be a linear function of the spray mass flux. In particular, the mean droplet velocity in Case 1 is much larger than those in Cases 2 and 3. The heat transfer coefficient for Case 1 is the smallest because the mass flux is smallest. This clearly demonstrates that spray mass flux, not the droplet velocity, is the dominant heat transfer factor in spray cooling, which is also consistent with the experimental findings in [32, 33].

In the non-boiling (or the single-phase) regime, it has been demonstrated [7] that single-phase convection, in a thin fluid-film formed on the target surface, is the primary heat transfer mechanism. However, thin fluid-film evaporation may occur, as evident in Figure 4, which shows a small amount of vapour near the targeted surface, playing only a minor role in the overall heat transfer. Compared with (conventional) forced convection, the enhanced heat transfer of spray cooling in the non-boiling regime is mainly derived from the discrete random nature of droplets disrupting the thin fluid-film. The disturbances due to impinging droplets are clearly evident in Figure 5 which shows quite a random velocity distribution in the film. It can also be clearly seen that at larger spray mass flux, the velocity in the film increases correspondingly resulting in higher heat transfer.

The temperature distributions on the targeted surface are shown in Figure 6. It is clearly evident (as expected) that the surface temperature decreases with an increase in spray mass flux. This is because the heat transfer coefficient is higher at larger spray mass flux as shown in Figure 3 i.e. more heat is removed from the surface, leading to a lower surface temperature since the total heat flux supplied for all three cases is the same. Furthermore, it can be seen that the surface temperature near to the centre is slightly lower but increases slowly away from the centre, with a maximum temperature difference of less than 2ºC between the centre and the edge. The low temperature region on the targeted surface is likely to stem from more droplets impinging on this area. This argument is supported by the higher induced gaseous velocity in the centre region owing to droplet motion with higher mass flux, as shown in Figure 7.

Figure 8 shows fluid film thickness on the target surface. It can be seen that the film thickness increases with the spray mass flux, i.e. a thicker film is formed on the target surface at higher spray mass flux. The velocity in the fluid film increases at higher spray mass flux as shown in Figure 5 but is not large enough to remove the increased fluid mass owing to more droplets arriving at the surface at higher spray mass flux resulting in an increase in film thickness. When the fluid film becomes ‘thick’, heat transfer from film evaporation reduces. But as shown in Figure 3 the heat transfer coefficient increases linearly with the spray mass flux. This strongly supports the argument that single-phase convection within the thin fluid film formed on the target surface, is the primary heat transfer mechanism [7]. Fluid film evaporation only plays a minor role in the overall heat transfer as already discussed.

4. CONCLUSIONS

This paper has described a numerical study to predict heat transfer in the non-boiling regime between a hot surface and impinging full-cone spray of water at atmospheric pressure. Coupled CFD-CHT simulations have been used to predict the fluid flow and heat transfer for

three different spray conditions. Spray breakup, wall-impingement, film formation, and both droplet and film evaporation have been simulated in a Lagrange-Eulerian framework. The predicted heat transfer coefficients are in good agreement with published experimental data. The key findings of the study are:

- The spray mass flux, not the droplet velocity, is the dominant factor for heat transfer in spray cooling. Both numerical prediction and experimental data show heat transfer coefficient as a linear function of spray mass flux.
- Single-phase convection within the thin fluid film is the primary heat transfer mechanism whereas film evaporation plays only a minor role in the overall heat transfer. Heat transfer by spray cooling in the non-boiling regime stems mainly from the discrete random nature of droplets disrupting the thin fluid film.
- The velocity distribution in the film, and the film thickness, are far from uniform on the target surface owing to the disturbance caused by impinging droplets.
- The spatial variation in surface temperature within the film is almost uniform with a maximum difference of less than 2^0C between the temperature in the centre region and the temperature near to the edge. A lower temperature in the centre region stems from a greater number of droplets impinging on the centre.

Acknowledgments

The authors wish to acknowledge funding support for this project from the EPSRC under Contract Number: EP/M005755/1. The technical support is also acknowledged of colleagues at Ford Dunton UK and Dearborn USA, Denso Italy, and the Ricardo Technical Centre Shoreham, UK.

References

[1] C. H. Amon, J. Murthy, S. C. Yao, S. Narumanchi, C.-F. Wu, and C.-C. Hsieh, “MEMS-enabled thermal management of high-heat-flux devices EDIFICE: embedded droplet impingement for integrated cooling of electronics,” *Exp. Therm. Fluid Sci.*, vol. 25, no. 5, pp. 231–242, 2001.

[2] M. Visaria and I. Mudawar, “Theoretical and experimental study of the effects of spray inclination on two-phase spray cooling and critical heat flux,” *Int. J. Heat Mass Transf.*, vol. 51, no. 9, pp. 2398–2410, 2008.

[3] I. Mudawar, “Assessment of High-Heat-Flux Thermal,” vol. 24, no. 2, pp. 122–141, 2001.

[4] J. Yang, L. C. Chow, and M. R. Pais, “Nucleate Boiling Heat Transfer in Spray Cooling,” *J. Heat Transfer*, vol. 118, no. 3, pp. 668–671, 1996.

[5] and M. R. P. L. C. Chow, M. S. Sehmbey, “High Heat Flux Spray Cooling,” *Annu. Rev. Heat Transf.*, vol. 8, pp. 291–317, 1997.

[6] K. Oliphant, B. W. Webb, and M. Q. McQuay, “An experimental comparison of liquid jet array and spray impingement cooling in the non-boiling regime,” *Exp. Therm. Fluid Sci.*, vol. 18, no. 1, pp. 1–10, 1998.

[7] J. Kim, “Spray cooling heat transfer: the state of the art,” *Proceedings of the 2006 International Conference on Boiling Heat Transfer*. 2006.

[8] M. Monde, “Critical Heat Flux in Saturated Forced Convection Boiling on a Heated Disk With an Impinging Jet,” *J. Heat Transfer*, vol. 109, no. 4, p. 991, 1987.

[9] I. Mudawar and W. S. Valentine, “Determination of the local quench curve for spray-cooled metallic surfaces,” *J. Heat Treat.*, vol. 7, no. 2, pp. 107–121, 1989.

[10] K. A. Estes and I. Mudawar, “Correlation of sauter mean diameter and critical heat flux for spray cooling of small surfaces,” *Int. J. Heat Mass Transf.*, vol. 38, no. 16, pp. 2985–2996, 1995.

[11] I. Mudawar, K. a. A. Estes, K. A. E. I. Mudawar, I. Mudawar, K. a. A. Estes, K. A. E. I. Mudawar, I. Mudawar, and K. a. A. Estes, “Optimizing and Predicting CHF in Spray Cooling of a Square Surface,” *J. Heat Transfer*, vol. 118, no. 3, p. 672, 1996.

[12] R.-H. Chen, L. C. Chow, and J. E. Navedo, “Effects of spray characteristics on critical heat flux in subcooled water spray cooling,” *Int. J. Heat Mass Transf.*, vol. 45, no. 19, pp. 4033–4043, 2002.

[13] M. Visaria and I. Mudawar, “A Systematic Approach to Predicting Critical Heat Flux for Inclined Sprays,” *J. Electron. Packag.*, vol. 129, no. 4, p. 452, 2007.

[14] A. G. Pautsch and T. A. Shedd, “Spray impingement cooling with single- and multiple-nozzle arrays. Part I: Heat transfer data using FC-72,” *Int. J. Heat Mass Transf.*, vol. 48, no. 15, pp. 3167–3175, 2005.

[15] E. A. Silk, E. L. Golliher, and R. Paneer Selvam, “Spray cooling heat transfer: Technology overview and assessment of future challenges for micro-gravity application,” *Energy Convers. Manag.*, vol. 49, no. 3, pp. 453–468, 2008.

[16] J. J. Nijdam, B. Guo, D. F. Fletcher, and T. A. G. Langrish, “Lagrangian and Eulerian models for simulating turbulent dispersion and coalescence of droplets within a spray,” *Appl. Math. Model.*, vol. 30, no. 11, pp. 1196–1211, 2006.

[17] M. Rahman, R. Mead, C. Hong, L. Lin, and R. Ponnappan, “Numerical Analysis of Spray Nozzle for Predicting Spray Cone Angle and Pressure Drop,” in *2nd International Energy Conversion Engineering Conference*, 2004.

[18] G. Tryggvason, B. Bunner, A. Esmaeeli, D. Juric, N. Al-Rawahi, W. Tauber, J. Han, S. Nas, and Y.-J. Jan, “A Front-Tracking Method for the Computations of Multiphase Flow,” *J. Comput. Phys.*, vol. 169, no. 2, pp. 708–759, 2001.

[19] D. W. Stanton and C. J. Rutland, “Multi-dimensional modeling of thin liquid films and spray-wall interactions resulting from impinging sprays,” *Int. J. Heat Mass Transf.*, vol. 41, no. 20, pp. 3037–3054, 1998.

[20] S. Sarkar and R. P. Selvam, “Direct Numerical Simulation of Heat Transfer in Spray Cooling Through 3D Multiphase Flow Modeling Using Parallel Computing,” *J. Heat Transfer*, vol. 131, no. 12, p. 121007, 2009.

[21] C. X. Bai, H. Rusche, and A. D. Gosman, “MODELING OF GASOLINE SPRAY IMPINGEMENT,” *At. Sprays*, vol. 12, no. 1–3, pp. 1–28, 2002.

[22] M. Jafari, “Analysis of heat transfer in spray cooling systems using numerical simulations,” University of Windsor, 2014.

[23] R. M. Youssef, “Modeling the Effect of a Spray on a Liquid Film on a Heated Surface,” 2007.

[24] K. Meredith, Y. Xin, and J. de Vries, “A Numerical Model for Simulation of Thin-Film Water Transport over Solid Fuel Surfaces,” *Fire Saf. Sci.*, vol. 10, pp. 415–428, 2011.

[25] S. Jafari, J. F. Dunne, M. Langari, Z. Yang, J.-P. Pirault, C. A. Long, and J. Thalackottore Jose, “A review of evaporative cooling system concepts for engine thermal management in motor vehicles,” *Proc. Inst. Mech. Eng. Part D J. Automob. Eng.*, Nov. 2016.

[26] M. Ciofalo, I. Di Piazza, and V. Brucato, “Investigation of the cooling of hot walls by liquid water sprays,” *Int. J. Heat Mass Transf.*, vol. 42, no. 7, pp. 1157–1175, 1999.

[27] D. Kalantari, “Characterization of liquid spray impact onto walls and films,” 2006.

[28] N. Karwa, S. R. Kale, and P. M. V Subbarao, “Experimental study of non-boiling heat transfer from a horizontal surface by water sprays,” *Exp. Therm. Fluid Sci.*, vol. 32, no. 2, pp. 571–579, 2007.

[29] *STAR-CCM+ User Guide*, Version 11. CD-adapco, 2016.

[30] D. B. LAUNDER, B. E., & SPALDING, *Lectures in Mathematical Models of Turbulence. London: Academic Press, 1972.* London, 1972.

[31] W. R. Ranz, W.E., and Marshall, “Evaporation from drops Parts I and II,” *Chem. Eng. Prog.*, vol. 48, no. 3, pp. 141–180, 1952.

[32] Y. Wang, M. Liu, D. Liu, and K. Xu, “Heat Flux Correlation for Spray Cooling in the Nonboiling Regime,” *Heat Transf. Eng.*, vol. 32, no. 11–12, pp. 1075–1081, Oct. 2011.

[33] S. Freund, A. G. Pautsch, T. A. Shedd, and S. Kabelac, “Local heat transfer coefficients in spray cooling systems measured with temperature oscillation IR thermography,” *Int. J. Heat Mass Transf.*, vol. 50, no. 9, pp. 1953–1962, 2007.

FIGURE CAPTIONS

Figure 1. Flow domain and boundary conditions.

Figure 2. Views of computational grid on domain boundaries (left) and a central section (right).

Figure 3. Variation of heat transfer coefficient with mass flux.

Figure 4. Vapour mass fraction; a) case 1, G=3.5 kg/m^{2}s, b) case 2, G=7.5 kg/m^{2}s, c) b) case 3, G=9.5 kg/m^{2}s.

Figure 5. Film velocity: a) case 1, G=3.5 kg/m^{2}s, b) case 2, G=7.5 kg/m^{2}s, c) case 3, G=9.5 kg/m^{2}s.

Figure 6. Temperature on the target surface: a) case 1, G=3.5 kg/m^{2}s, b) case 2, G=7.5 kg/m^{2}s, c) b) case 3, G=9.5 kg/m^{2}s.

Figure 7. Induced velocity field in the chamber a central section: a) case 1, G=3.5 kg/m^{2}s, b) case 2, G=7.5 kg/m^{2}s, c) b) case 3, G=9.5 kg/m^{2}s.

Figure 8. Film thickness: a) case 1, G=3.5 kg/m^{2}s, b) case 2, G=7.5 kg/m^{2}s, c) case 3, G=9.5 kg/m^{2}s.

LIST OF FIGURES

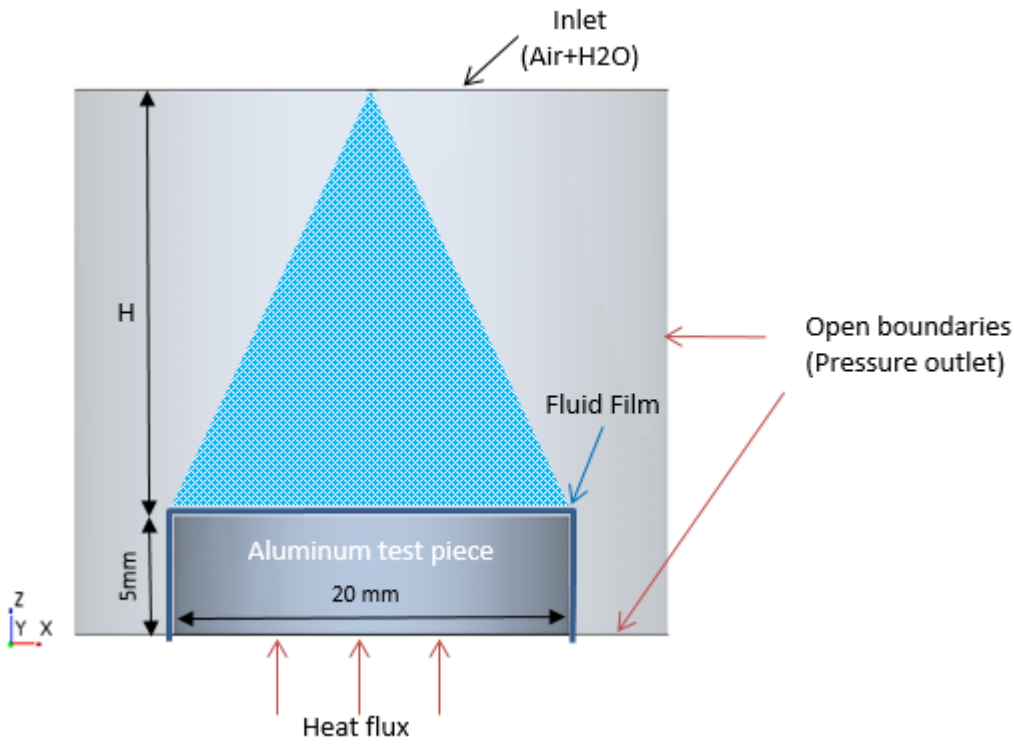

Figure 1. Flow domain and boundary conditions

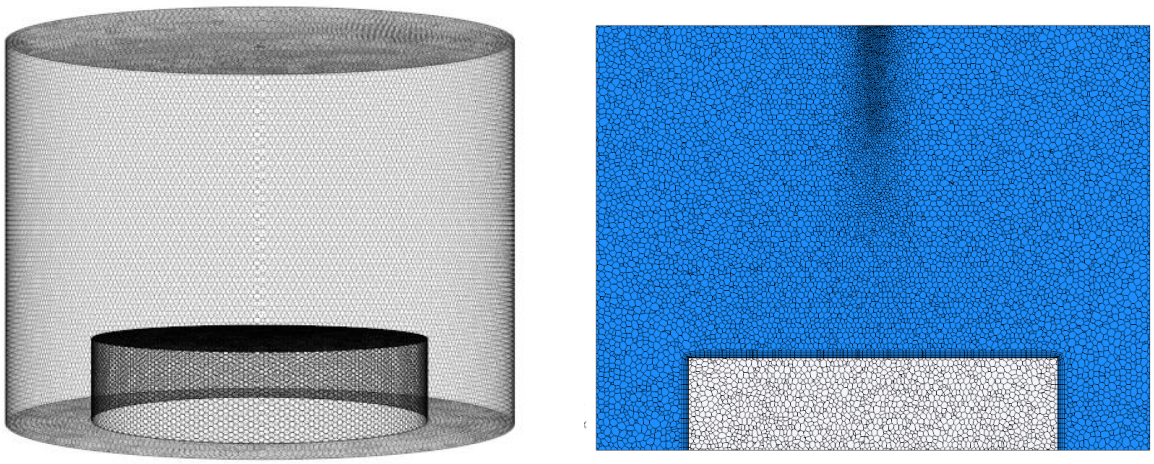

Figure 2. Views of computational grid on domain boundaries (left) and a central section (right).

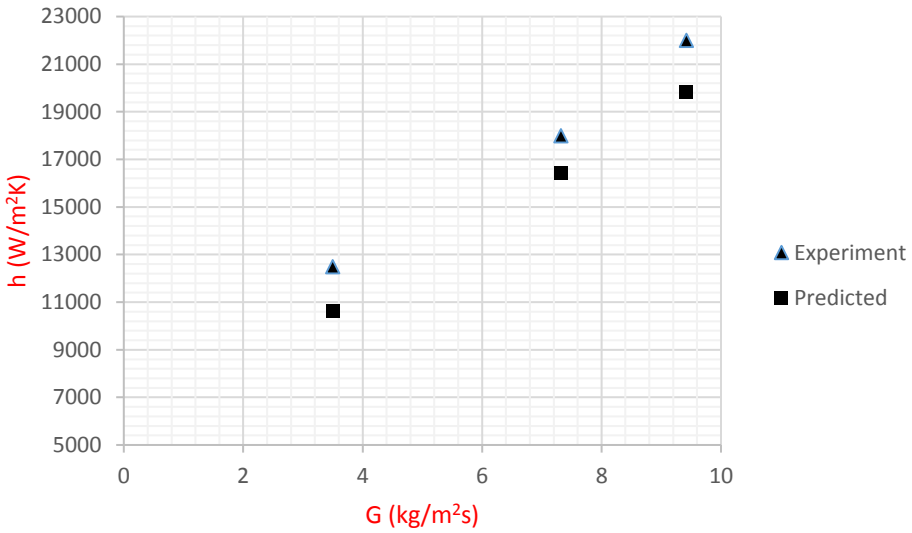

Figure 3. Variation of heat transfer coefficient with mass flux.

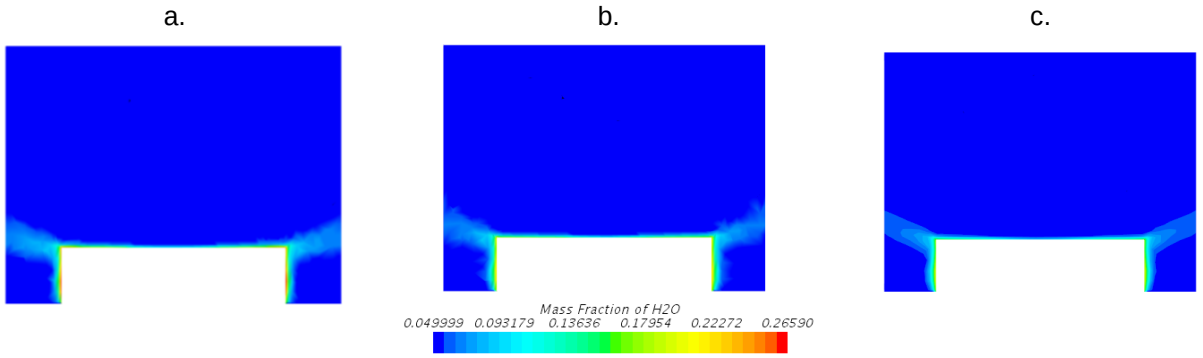

Figure 4. Vapour mass fraction; a) case 1, G=3.5 kg/m²s, b) case 2, G=7.5 kg/m²s, c) b) case 3, G=9.5 kg/m²s.

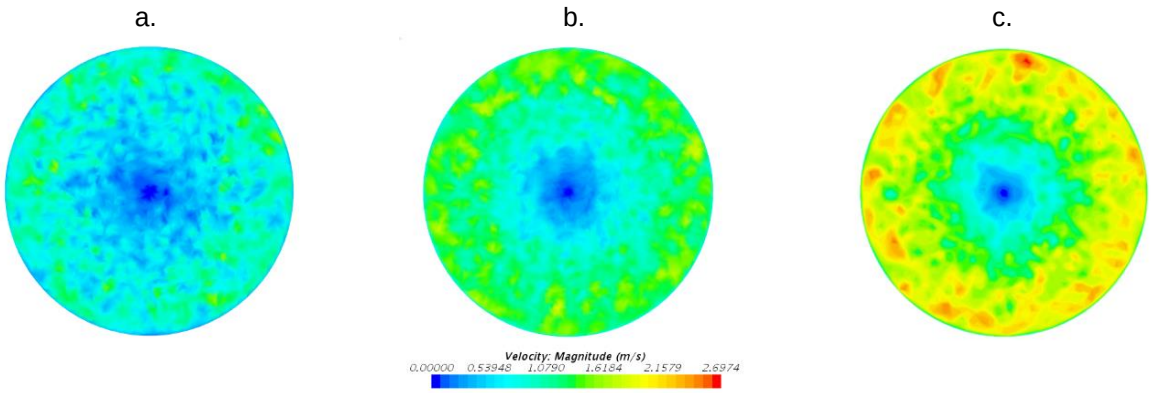

Figure 5. Film velocity: a) case 1, G=3.5 kg/m²s, b) case 2, G=7.5 kg/m²s, c) case 3, G=9.5 kg/m²s.

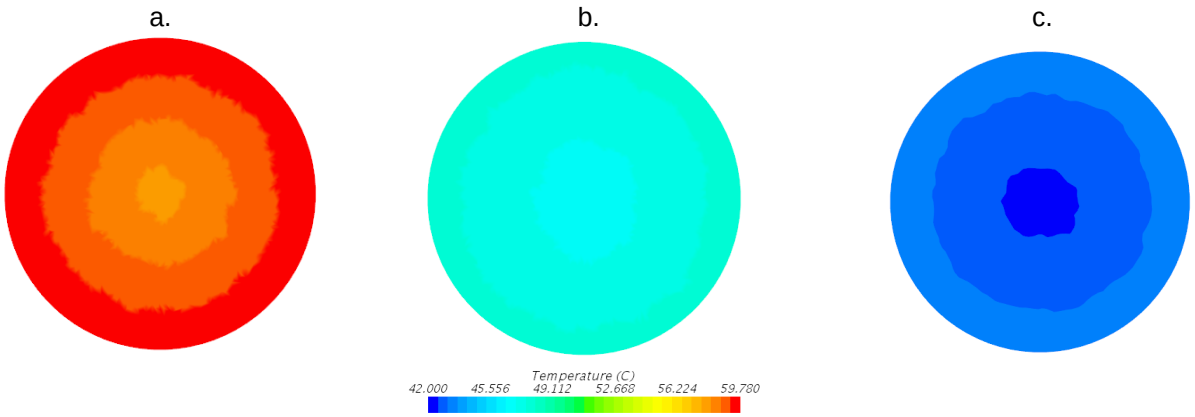

Figure 6. Temperature on the target surface: a) case 1, G=3.5 kg/m^{2}s, b) case 2, G=7.5 kg/m^{2}s, c) b) case 3, G=9.5 kg/m^{2}s.

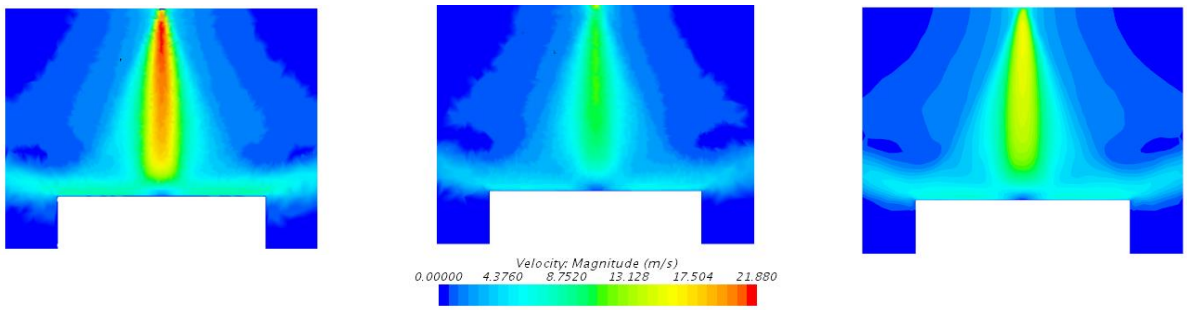

Figure 7. Induced velocity field in the chamber a central section: a) case 1, G=3.5 kg/m^{2}s, b) case 2, G=7.5 kg/m^{2}s, c) b) case 3, G=9.5 kg/m^{2}s.

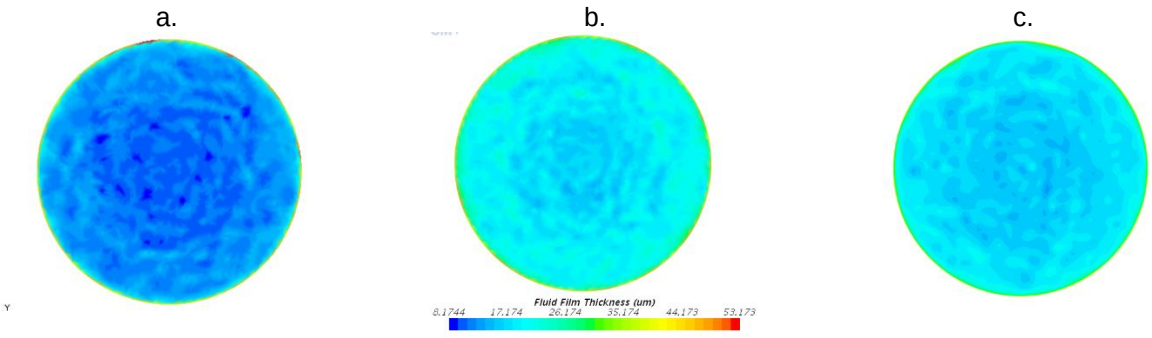

Figure 8. Film thickness: a) case 1, G=3.5 kg/m^{2}s, b) case 2, G=7.5 kg/m^{2}s, c) case 3, G=9.5 kg/m^{2}s.